Chemical Engineering Journal 309 (2017) 577–587

Contents lists available at ScienceDirect

Chemical Engineering Journal

journal homepage: www.elsevier.com/locate/cej

Adsorption of aromatic organoarsenic compounds by ferric and manganese binary oxide and description of the associated mechanism

Tista Prasai Joshi [a,c], Gong Zhang [b], William A. Jefferson [a], Aleksandr V. Perfilev [a,d], Ruiping Liu [a,c,*], Huijuan Liu [b,c], Jiuhui Qu [a,c]

[a] Key Laboratory of Drinking Water Science and Technology, Research Center for Eco-Environmental Sciences, Chinese Academy of Sciences, Beijing 100085, China
[b] State Key Laboratory of Environmental Aquatic Chemistry, Research Center for Eco-Environmental Sciences, Chinese Academy of Sciences, Beijing 100085, China
[c] University of Chinese Academy of Sciences, Beijing 100049, China
[d] Institute of Chemistry, Far-Eastern Branch of Russian Academy of Sciences, Vladivostok 690022, Russian Federation

HIGHLIGHTS

- FMBO shows higher removal capacity towards p-ASA and ROX than FeOOH and MnO_2.
- Adsorption of p-ASA and ROX onto FMBO, FeOOH, and MnO_2 is more favorable at pH 4.0.
- Heterogeneous oxidation involves in the adsorption of p-ASA onto FMBO and MnO_2.
- The synergism of Fe- and Mn-oxide dominates the high adsorption capacity of FMBO.

GRAPHICAL ABSTRACT

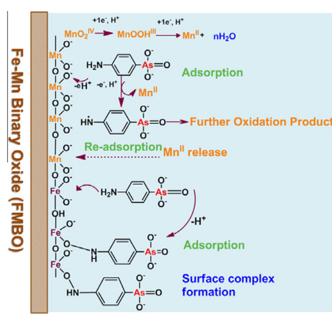

ARTICLE INFO

Article history:
Received 8 August 2016
Received in revised form 17 October 2016
Accepted 18 October 2016
Available online 19 October 2016

Keywords:
FMBO
FeOOH
MnO_2
Para arsanilic acid
Roxarsone
Heterogeneous oxidation

ABSTRACT

The aromatic organoarsenic compounds including p-arsanilic acid (p-ASA) and roxarsone (ROX) used as feed additives in the poultry appear to be excreted with no chemical structural change, tending to environmental release of inorganic arsenic. Thus, effective removal and understanding the mechanism of organoarsenic compounds are of significant urgency. We herein investigated the interactions of organoarsenic compounds with ferric and manganese binary oxide (FMBO) to investigate their adsorption efficiency and mechanism, whereas ferric oxide (FeOOH), and manganese oxide (MnO_2) were also studied for the comparison. The maximum adsorption capacities (Q_{max}) of FMBO towards p-ASA and ROX were determined to be 0.52 and 0.25 mmol g^{-1} (pH = 7.5). FeOOH and MnO_2 showed lower adsorption capability, the corresponsive $Q_{max,\ p\text{-}ASA}$ were 0.40 and 0.33 mmol g^{-1} and $Q_{max,\ ROX}$ were 0.08 and 0.07 mmol g^{-1}, respectively. The elevated pH inhibited the adsorption onto the adsorbents owing to the increased repulsive forces; the $Q_{max,\ p\text{-}ASA}$ and $Q_{max,\ ROX}$ onto FMBO increased to 0.79 and 0.51 mmol g^{-1} at pH 4.0. Based on results of UV–vis spectra, UPLC-ICP-MS, FTIR, and XPS, the synergistic effect of heterogeneous oxidation and adsorption was the core for efficient aqueous removal of p-ASA by FMBO. Manganese oxide showed significant oxidation of p-ASA, while adsorption process was observed in ferric oxide and this effect also involves in the adsorption of ROX. Results herein extended the knowledgebase on organoarsenic species adsorption to Fe/Mn oxides, are important for potential engineering treatment application and help us to understand reactions at the interfacial level.

1. Introduction

Aromatic organoarsenic, e.g., 4-aminophenylarsonic acid (para-arsanilic acid, p-ASA) and 4-hydroxy-3-nitrophenylarsonic acid

* Corresponding author at: Key Laboratory of Drinking Water Science and Technology, Research Center for Eco-Environmental Sciences, Chinese Academy of Sciences, Beijing 100085, China.
E-mail address: liuruiping@rcees.ac.cn (R. Liu).

http://dx.doi.org/10.1016/j.cej.2016.10.084
1385-8947/© 2016 Published by Elsevier B.V.

(Roxarsone, ROX), are widely used as feed additives of broiler chickens to control coccidial intestinal parasites, improve feed efficiency, stimulate rapid growth, and improve pigmentation [1,2]. The arsenic content in poultry manure is as high as over 40 mg kg^{-1} [3]. The use of poultry litter as organic fertilizer transfers from 'point' to 'non-point' source pollution, and increases the risk of organoarsenic contamination towards soils and groundwater accordingly [4]. Upon entering environments, organoarsenic tends to transform into more mobile toxic inorganic arsenite [As(III)] and arsenate [As(V)] by microbial activities [1,5,6]. The removal of organoarsenic prior to its entering environments is of crucial importance to control their environmental risk.

Adsorption exhibits the advantageous of simple operation, high efficiency, low cost, and is practically valuable for organoarsenic removal [7]. Many adsorbents have been developed for the removal of inorganic arsenic such as multi-wall carbon nanotubes (MWCNTs) [8], biosorbent (scales of *Cyprinus carpio*) [9], zeolitic imidazolate frameworks [10], copper impregnated natural mineral tufa [11], and ferrihydrite [12]. However, the adsorbents for organoarsenic removal are relatively rare. There have been reported several adsorbents, i.e., birnessite [13], mesoporous zeolitic imidazolate framework-8 [14], metal-organic frameworks [15], MWCNTs [16,17], chitosan-based copolymers [18], iron and aluminum oxides [19], and titanium oxides [20] for the removal of organoarsenic (Table S1). However, their practical application is limited due to the difficulty in large scale production. Previous studies in our research group using ferric and manganese binary oxide (FMBO), for arsenic(III) removal revealed interesting results and led to development of engineering applications [21]. This result inspired us the effectively converted the chemical structure of the organoarsenic was conducive to entire removal process. In FMBO, manganese (Mn) oxide shows oxidative and adsorptive capacities towards aromatic amines [22]. Then, the low cost iron oxides have been exhibited the good adsorption performances towards aromatic organoarsenic [23]. Thus, we speculated if the same synergistic effects of mixed Mn(IV)/Fe(III) oxide could provide similar adsorption capacity for organoarsenic species.

In this study, we selected two aromatic organoarsenic compounds of p-ASA and ROX with different reductive dissolution effect, investigated removal efficiency of FMBO, and adsorption mechanism. The macroscopic adsorption experiments such as adsorption kinetics, adsorption isotherms, and pH effects were conducted. After that, removal mechanisms of organoarsenic compound on the interfacial of FMBO were analyzed by UV–vis scan, UPLC-ICP-MS, and microscopic characterization techniques such as FTIR and X-ray photoelectron spectroscopy (XPS). Finally, the dominant interfacial reactions involved in the adsorption of p-ASA and ROX onto the adsorbents were proposed accordingly.

2. Experiments

2.1. Materials and analysis methods

The p-ASA (>98%) and ROX (>98%) were respectively purchased from TCI Chemicals Co. and Sinopharm Chemical Reagent Co. Table 1 illustrates their dominant physicochemical characteristics and their species distribution over a wide pH range. All other analytical grade chemicals were purchased from Beijing Chemical Co. The stock solutions of p-ASA and ROX (15 mmol L^{-1}) and working solutions of different concentrations were prepared using Milli-Q deionized water (18.2 MΩ-cm). FMBO with different Fe/Mn molar ratios were prepared at room temperature, among of which the ratio of 3:1 was the optimal one. The preparation of FMBO, FeOOH, and MnO_2 followed the methods as described in previous studies [21,24,25], and the detailed procedures are illustrated in the supporting information (Text S1).

2.2. Adsorption experiments

Sodium perchlorate ($NaClO_4{\cdot}H_2O$) at 0.01 M was used to maintain the background ionic strength. pH was adjusted during adsorption using 0.1 M NaOH and 0.1 M HNO_3 to achieve pH variation in the range of ±0.1. All the batch experiments were proceeded in triplicate at the same time. Blank control experiments without the addition of adsorbents confirmed that no adsorption occurred on the glass vial wall. Control experiments only adsorbents without p-ASA/ROX indicated that no loss of Fe and Mn from adsorbents.

In adsorption kinetic experiments, the initial concentrations of p-ASA ($[\text{p-ASA}]_0$) and ROX ($[\text{ROX}]_0$) were 0.15 mmol L^{-1}, and adsorbents doses were 0.2 g L^{-1}. Batch adsorption experiments were conducted in a beaker with magnetic stirrer (350 rev min^{-1}) at pH 7.5 ± 0.1 in room temperature. Aliquots (~5 mL) were taken from the suspension at different time intervals of 0.016, 0.08, 0.25, 0.5, 1.0, 1.5, 2.0, 3.0, 5.0, 8.0, 13.0, 23.0, 37.0, 55.0, and 79.0 h. The adsorbent capacity (q_t) was calculated according to Eq. (1) as follows:

$$q_t = \frac{(C_0 - C_t)V}{m} \tag{1}$$

where q_t is adsorption capacity in mmol g^{-1}, C_0 and C_t are the concentrations of p-ASA and ROX (mmol L^{-1}) before and after adsorption, m is the amount of the adsorbent used (g), and V is the volume of the initial solution (L).

The removal rate (%) was calculated according to Eq. (2):

$$\text{Removal }\% = \frac{C_0 - C_e}{C_0} \times 100 \tag{2}$$

where C_0 is the initial concentrations of the p-ASA and ROX and C_e are the final concentration of p-ASA and ROX, respectively.

In adsorption isotherms experiments, the concentrations of $[\text{p-ASA}]_0$ and $[\text{ROX}]_0$ were in the range from 0.02 to 1.0 mmol L^{-1} with the adsorbents doses of 0.25 g L^{-1}. Adsorption experiments were conducted in 50 mL polypropylene tubes with 40 mL solution at pH 7.5 ± 0.1, and the tubes were kept on an end-over-end shaker set at 40 rpm for 24.0 h in room temperature to achieve equilibrium. To investigate the effects of pH on adsorption, similar procedures were used except that initial pH was adjusted to desired values from 4.0 to 9.0 prior to the addition of adsorbents.

The equilibrium uptake (q_e, mmol g^{-1}) of an adsorbent towards an adsorbate is calculated using Eq. (3).

$$q_e = \left[\frac{(C_0 - C_e)XV}{M}\right] \tag{3}$$

where C_0 is the initial concentration (M) of the adsorbate, C_e is the equilibrium concentration (M) of the adsorbate, V is the volume (L) of the adsorbate, and M (g) is dosage level of the adsorbent employed.

2.3. Characterization and analytical methods

The powder X-ray diffraction patterns (XRD) of FMBO, FeOOH, and MnO_2 were determined using an X'Pert 3040-PRO Powder diffractometer machine (PANalytical Co.). Data were collected at 40 keV using a graphite curved crystal monochromator between 10° and 90° 2θ in 0.02° steps. The specific surface area (S_{BET}), pore volume, and pore size distribution were measured by nitrogen adsorption method with a Micrometrics ASAP 2020 HD88 surface area analyzer (Micrometrics Co. USA). The morphology of the adsorbents was observed under scanning electron microscope

Table 1
Physicochemical characteristics of p-ASA and ROX.

Adsorbate	Molecular structure*	Speciation	Molecular formula	Molecular weight ($g\ mol^{-1}$)
4-Aminophenylarsonic acid Para arsanilic acid p-ASA	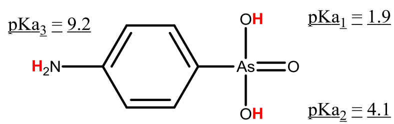	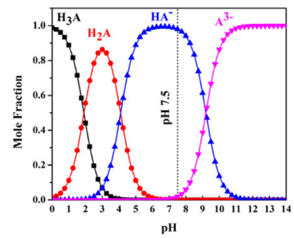	$C_6H_8NO_3As$	217.05
4-Hydroxy-3-nitrophenylarsonic acid Roxarsone ROX	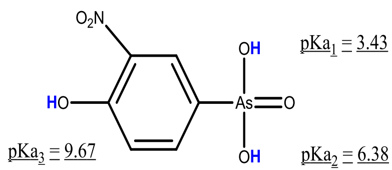	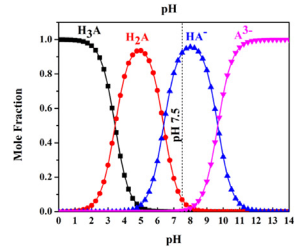	$C_6H_8NO_6As$	263.04

* pK_a values are referred to [19].

(SEM) with an EDAX KEVEX level 4 (Hitachi S-3500N, Japan). The electrokinetic potential (ζ-potential) was measured by a Zetasizer 2000 Zeta Potential Analyzer (Malvern Co., UK). Fourier transform infrared (FTIR) spectra of adsorbents before and after adsorption were recorded on a TENSOR 27 BRUKER, Germany spectrometer. X-ray photoelectron spectroscopy (XPS) data were collected for the analysis of elemental composition and their valence states by an ESCA-Lab-220i-XL spectrometer (Shimadzu Co., Japan) with monochromatic Al Kα radiation (225 W, 15 mA, 15 kV).

After adsorption, samples were filtered through 0.45-μm membrane filters for the analysis of arsenic (As) species, manganese (Mn), and oxidation intermediates. The concentrations of arsenic (As) species and manganese (Mn) were measured by an inductively coupled plasma optical emission spectroscopy (ICP-OES-710 Agilent Technology, USA). UV–vis spectra were collected using UV–vis spectrophotometer (U-3010; Hitachi High technologies Co., Japan). Wavelength scan of p-ASA and ROX was monitored in the ranges of 190–550 nm using UV–vis spectrophotometer over a wide range of pH (2.0–10.0). The oxidative intermediates were detected by ultra-high performance liquid chromatography inductively coupled plasma mass spectroscopy (UPLC-ICP-MS, Thermo Scientific-iCAP-Q) with a PRPX100 anion-exchange column (Hamilton Company) at 298 K [26]. The mobile phase solution was prepared by dissolving $(NH_4)_2HPO_4$ (1.36 g) and NH_4NO_3 (0.8004 g) into 1 L of Milli-Q deionized water (18.2 MΩ-cm). The pH was adjusted to 6.2 by adding 1 M HNO_3. It was passed through the column at 1.0 mL min^{-1}. The mass spectrum (MS) detector was used to observe the peak of the arsenic species at m/z 75 through the "time resolved analysis" mode [27]. The concentration of arsenic (As) species was identified on the basis of retention time of the standard solution of As (III), As (V), and p-ASA.

3. Results and discussion

3.1. Characterization of adsorbents

The XRD pattern of FMBO, FeOOH, and MnO_2 with 2θ ranging from 10° to 90°, as illustrated in Fig. S1A indicated that these adsorbents were in amorphous form except that only a few crystalline peaks were detected. The amorphous adsorbents have high S_{BET} with plentiful active surface sites [21]. Additionally, the nitrogen adsorption and desorption isotherms of FMBO and MnO_2 were observed to be type II with H3 hysteresis and FeOOH was type IV isotherms with H2 hysteresis (Fig. S1B). S_{BET} values of FMBO, FeOOH, and MnO_2 were determined to be 216.1, 46.6, and 93.2 $m^2\ g^{-1}$, respectively in Table S2. SEM images of FMBO, FeOOH, and MnO_2 indicated many aggregated small particles with a porous structure (Fig. S1C) and this is in accordance with previous study [21]. The ζ-potential of three adsorbents decreased with elevated pH (Fig. S2), and the isoelectric point (pH_{iep}) was determined to be 5.4, 5.6, and ~2.0 for FMBO, FeOOH, and MnO_2, respectively. The elemental composition of FMBO, FeOOH, and MnO_2 were determined by XPS technique as shown in Table 2. The atomic percentage (at.%) of Fe and Mn elements was found to be 16.86 at.% and 6.07 at.% in FMBO, the ratio of Fe–Mn was observed to be 2.8:1 (~3:1). The percentage of Fe and O elements was found to be 33.0 at.% and 66.92 at.% for FeOOH and Mn and O was observed to be 22.3 at.% and 55.2 at.% for MnO_2, respectively.

3.2. Macro-scopic adsorption behaviors of p-ASA and ROX onto applied adsorbents

3.2.1. Adsorption kinetics

Fig. 1 illustrates the adsorption of p-ASA and ROX by FMBO, FeOOH, and MnO_2 (mmol g^{-1}) as a function of time. The adsorption of p-ASA and ROX increased rapidly during the initial stage of 2.0 h, and after that, the slow decrease stage was observed. After 2.0 h contact time, the $q_{t,\ p\text{-}ASA}$ and $q_{t,\ ROX}$ on FMBO was observed to be 0.25 and 0.15 mmol g^{-1}, which was relative to 34.3% and 25.0% of their equilibrium adsorption after 79.0 h contact time (q_{eq}). FMBO showed more significant adsorption towards p-ASA and ROX than both FeOOH and MnO_2. The equilibrium adsorption of p-ASA ($q_{eq,\ p\text{-}ASA}$) and ROX ($q_{eq,\ ROX}$), was found to be 0.35 and 0.20 mmol g^{-1} for FMBO, 0.27 and 0.15 mmol g^{-1} for FeOOH, and 0.13 and 0.04 mmol g^{-1} for MnO_2, respectively. The more significant adsorption of p-ASA onto these adsorbents was observed as compared to that of ROX (Fig. S3).

The obtained data were further fitted with five kinetic models of pseudo-first-order, pseudo-second order, Elovich, power function, and intra particle diffusion models, Table S3 compared the fitted parameters. Elovich model was best fitted to describe the adsorption of p-ASA (R^2 = 0.98) and ROX (R^2 = 0.98) onto FMBO, indicated

Table 2
Elemental composition of p-ASA, ROX, FMBO, FeOOH, MnO_2 before and after p-ASA and ROX adsorption at pH 4.0 and 7.5.

S.N	Sample	Mn (at.%)	As (at.%)	N (at.%)	Fe (at.%)	O (at.%)	C (at.%)
1	p-ASA	0.0	9.48	8.24	0.0	21.16	61.10
2	ROX	0.0	8.23	7.01	0.0	36.38	48.36
3	FMBO	6.07	0.0	0.0	16.86	52.73	24.33
4	FMBO with p-ASA pH 4.0	3.45	3.67	3.95	11.41	41.66	35.83
5	FMBO with ROX pH 4.0	4.64	2.68	3.16	12.13	49.00	28.36
6	FMBO with p-ASA pH 7.5	4.28	1.34	1.64	9.78	40.73	42.20
7	FMBO with ROX pH 7.5	4.80	0.83	1.43	14.00	46.57	32.35
8	FeOOH	0.0	0.0	0.0	33.00	66.99	0.0
9	FeOOH with p-ASA pH 4.0	0.0	3.542	5.02	4.46	28.65	56.34
10	FeOOH with ROX pH 4.0	0.0	3.32	5.99	5.56	37.11	45.54
11	FeOOH with p-ASA pH 7.5	0.0	1.86	2.18	16.55	46.69	32.40
12	FeOOH with ROX pH 7.5	0.0	0.89	1.48	17.77	48.56	30.94
13	MnO_2	22.32	0.0	0.0	0.0	55.19	22.48
14	MnO_2 with p-ASA pH 4.0	11.15	3.81	4.16	0.0	34.49	46.37
15	MnO_2 with ROX pH 4.0	13.70	1.01	1.55	0.0	39.75	43.97
16	MnO_2 with p-ASA pH 7.5	22.52	0.79	0.72	0.0	50.95	24.99
17	MnO_2 with ROX pH 7.5	22.93	0.51	0.0	0.0	52.59	23.95

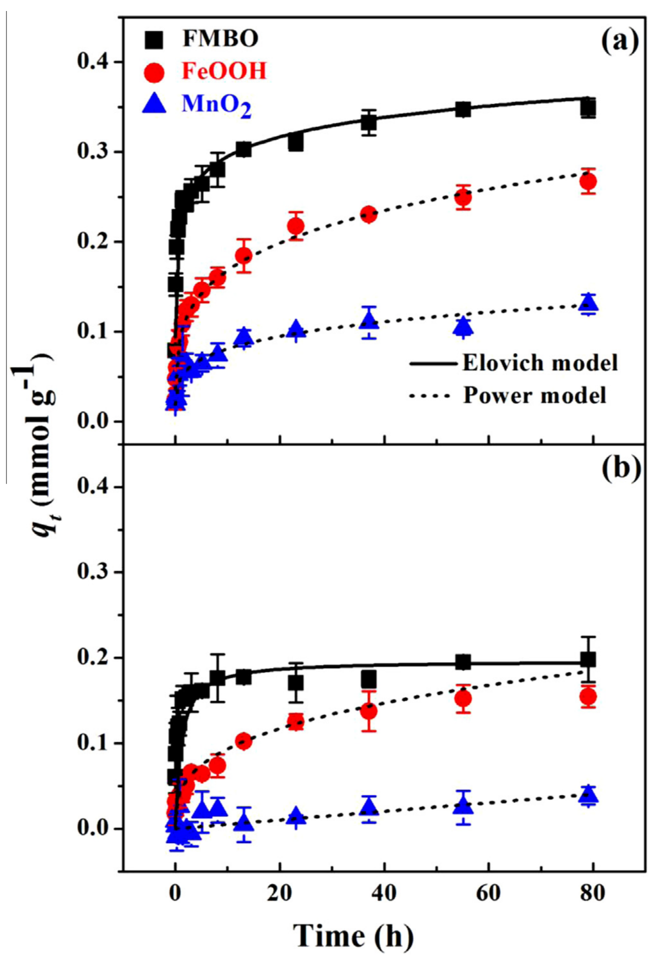

Fig. 1. Adsorption kinetics of (a) p-ASA and (b) ROX onto FMBO, FeOOH, and MnO_2. The lines through the data points represent the fitting by kinetics models, solid line (–) mean the Elovich model and dash lines (---) represent to the power model.

the occurrence of heterosphere diffusion reactions [28]. Comparatively, the adsorption of p-ASA and ROX onto FeOOH (R^2 = 0.99 and 0.98) and MnO_2 (R^2 = 0.99 and 0.71) was best fitted by the power function model. As for the power function model, FMBO showed higher the rate constant of k_4 than FeOOH and MnO_2 in Table S3, suggested the higher velocity in the adsorption of p-ASA and ROX onto FMBO than those onto the other adsorbents [29]. Additionally, the adsorption equilibrium was achieved within 20.0 h and thus 24.0 h contact time was applied in the following experiments.

3.2.2. Adsorption isotherms

The adsorption isotherms of p-ASA and ROX onto FMBO, FeOOH, and MnO_2 at pH 7.5 ± 0.1 are illustrated in Fig. 2. The maximum

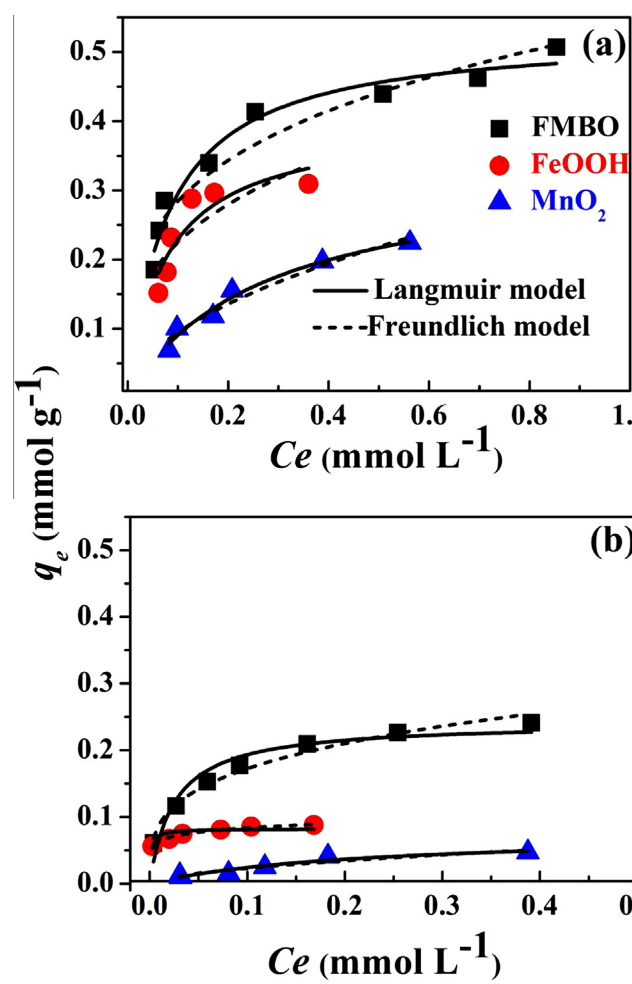

Fig. 2. Adsorption isotherms for the adsorption of (a) p-ASA and (b) ROX onto FMBO, FeOOH, and MnO_2 surfaces. Solid line (–) mean the Langmuir model and dash lines (----) represent to the Freundlich model.

adsorption capacity (Q_{max}) of FMBO towards p-ASA and ROX were determined to be 0.52 and 0.25 mmol g^{-1}. FeOOH and MnO_2 showed lower adsorption capability, and their corresponsive $Q_{max,\ p\text{-}ASA}$ were determined to be 0.40 and 0.33 mmol g^{-1} and $Q_{max,\ ROX}$ to be 0.08 and 0.07 mmol g^{-1}, respectively. As for the adsorption of antimony, FMBO also showed higher Q_{max} than the other two adsorbents [24] that showed higher adsorption capacity of FMBO towards antimony. The calculated $q_{e,\ cal}$ values are in accordance with the experimental values as expressed as q_e in Table S4.

These experimental data were further fitted by Langmuir and Freundlich isotherms to understand the adsorption processes. The Langmuir model was better than the Freundlich model to describe the adsorption of p-ASA onto FMBO, FeOOH, and MnO_2 and the R^2 values were determined to be 0.96, 0.78, and 0.96, respectively in Table S4. The adsorption of ROX onto FMBO and FeOOH was well fitted by Freundlich model with the R^2 values of 0.96 and 0.98, whereas that onto MnO_2 was better fitted by Langmuir model ($R^2 = 0.91$). Langmuir model is related to the monolayer sorption mechanism with homogeneous sorption energies, Freundlich model corresponds to the multilayer sorption sites and heterogeneous sorption energies [30,31].

The higher removal capacity of FMBO may be first attributed to the more adsorption sites available on FMBO surfaces than those on the surfaces of FeOOH and MnO_2, and S_{BET} results supported this assumption in Table S2. FMBO shows high removal capacity towards the organoarsenic and are potentially feasible for the removal of p-ASA and ROX in practice.

3.2.3. Effects of pH

Fig. 3 illustrates the adsorption of p-ASA and ROX onto these adsorbents over a wide pH range from 4.0 to 9.0, and the higher adsorption capability towards p-ASA and ROX on FMBO was also observed as compared to FeOOH and MnO_2. The adsorption of p-ASA and ROX was most significant at pH 4.0 and the elevated pH inhibited their adsorption on any adsorbent. The maximum adsorption of p-ASA onto FMBO, FeOOH, and MnO_2 at pH 4.0 was determined to be 0.79, 0.45, and 0.55 mmol g^{-1}, respectively. The corresponsive adsorption of ROX was relatively lower to be 0.51, 0.32, and 0.27 mmol g^{-1} for FMBO, FeOOH, and MnO_2. The obtained *qe* value of p-ASA and ROX onto FMBO, FeOOH, and MnO_2 at pH 7.0 was observed to be closely similar with the *qe* value of the adsorption isotherm at pH 7.5.pH significantly affected the species distribution of aromatic organoarsenic in Table 1 and the surface charge of adsorbents (Fig. S2). p-ASA and ROX with amphoteric nature predominantly exist as mono-anionic and di-anionic species at pH 7.5, the elevated pH favors their transformation to di-anionic species and decreases their adsorption accordingly. It was inferred that the protonated p-ASA and ROX are adsorbed more strongly onto adsorbents than the deprotonated ones [32].

The surface of adsorbents, which is denoted as ≡S—OH herein, is more positively-charged at lower pH due to the protonation Eq. (4), and this benefits the adsorption of negative p-ASA and ROX. At elevated pH above pH_{iep}, the deprotonation of ≡S—OH occurs and the negatively-charged surfaces are observed [33].

$$pH < pH_{iep} : \equiv S - OH + H_2O \rightarrow \equiv S - OH_2^+ + OH^- \text{ (Protonation)} \tag{4}$$

Additionally, the adsorption of aromatic organoarsenic may be attributed to the formation of inner-sphere complex on ≡S—OH [34]. In this case, the substitution of surface hydroxyl group (—OH) contributes to OH^- release [12] and the more significant adsorption was observed at lower pH accordingly [35]. At higher pH than pH_{iep}, i.e., 5.6 for FMBO, 5.4 for FeOOH, and ~2.0 for MnO_2, these adsorbents showed negative surfaces and the Coulombic repulsive force between organoarsenic and ≡S—OH was stronger at elevated pH (Fig. S4).

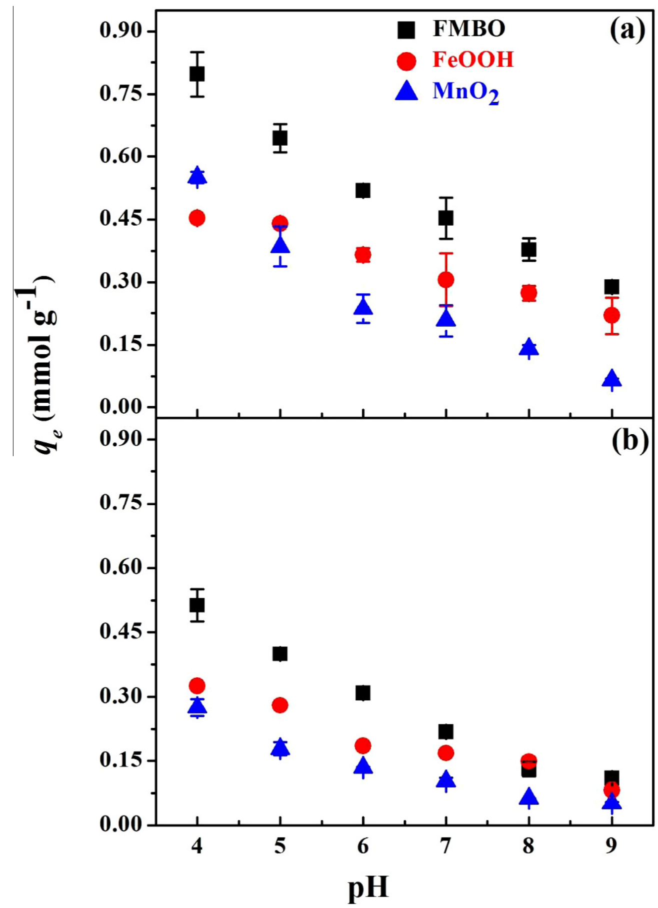

Fig. 3. Effect of pH on the adsorption of (a) p-ASA and (b) ROX onto FMBO, FeOOH, and MnO_2.

3.3. Removal mechanisms of p-ASA and ROX on the interfacial of FMBO

The macroscopic result supported that FMBO had superior adsorption performance to the aromatic organoarsenic compounds. Thus, to gain insight into the relationships between the surface of FMBO and aqueous organoarsenic is of great significance. Results of UV–vis spectra in the wavelength range from 190 to 550 nm corroborated the oxidation of organoarsenic by Mn(IV) (Fig. 4). At pH 7.5, p-ASA shows two absorption peaks at a wavelength 250 nm and 206 nm and ROX exhibits three peaks at wavelength of 400 nm, 244 nm, and 206 nm. The absorption peak at 250 nm associated with the aromatic ring within p-ASA, whereas that at 400 nm was related to the 4-nitrophenol group within ROX [36,37]. It was noted that their peak position may vary to some extent in different pH range (Fig. S5). After being adsorbed onto FMBO, the absorbance of p-ASA at 250 nm (A_{250nm}) decreased by 0.77 a.u, higher than that of 0.64 a.u for FeOOH, and 0.08 a.u for MnO_2, respectively (Fig. 4a, inset), which was in accordance with the highest adsorption of p-ASA was observed on FMBO. However, the broad distinctive peak of p-ASA, in the wavelength range from 300 to 400 nm, was observed to increase with prolonged contact time after being adsorbed on MnO_2. Meanwhile, there appeared a new peak at 310 nm (Fig. 4c, inset), attributed to the formation of the azophenylarsonic acid after the coupling of the oxidized p-ASA intermediates [13]. Comparatively, the absorbance at

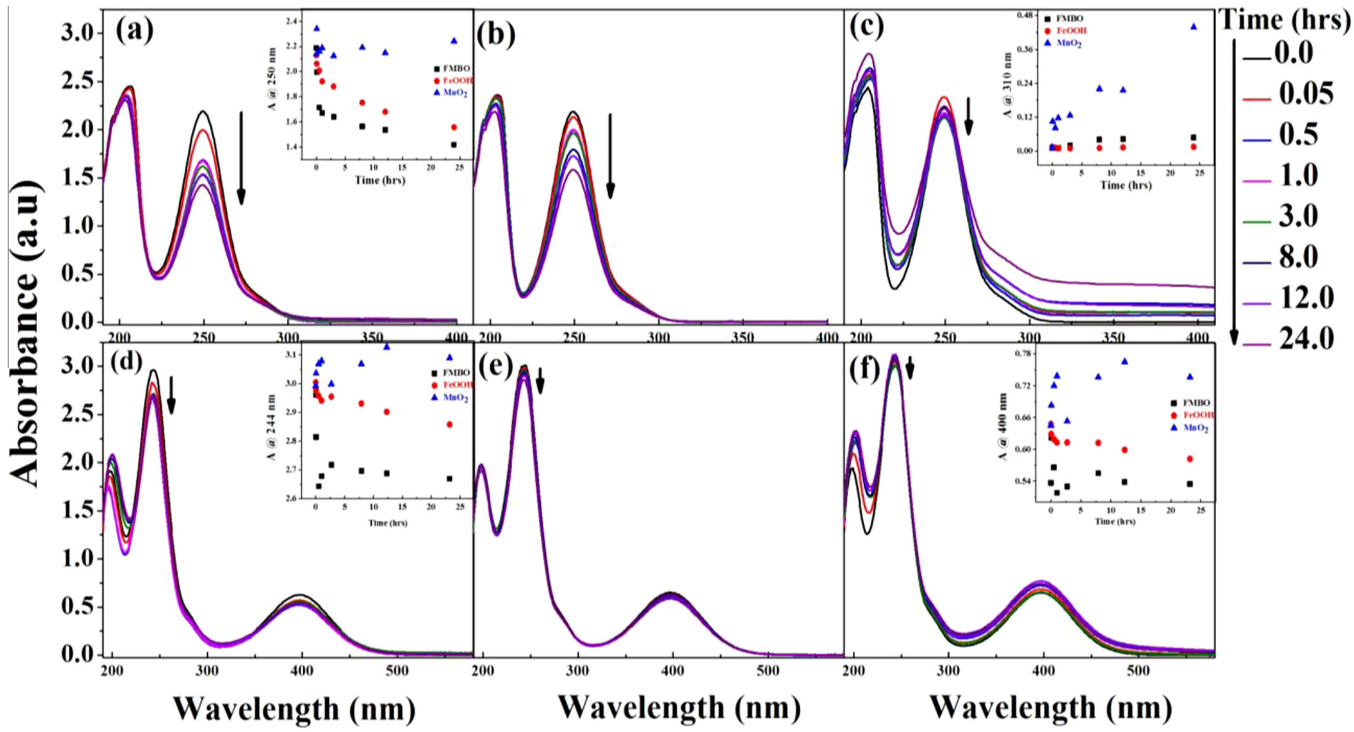

Fig. 4. Changes in UV–vis absorption spectra after the adsorption of (a, b, and c) p-ASA and (d, e, and f) ROX onto (a & d) FMBO, (b & e) FeOOH, and (c & f) MnO_2 at pH 7.5 (inset a, c, d, and f absorbance @ 250, @ 310, @ 244, and @ 400 nm, respectively).

310 nm (A_{310nm}) increased in lower extent after the adsorption of p-ASA on FMBO, while FeOOH with no oxidation efficacy cannot contribute to A_{310nm} increase even after 24.0 h contact time. The oxidative behaviors of Mn(IV) oxide within MnO_2 and FMBO occurred and showed effects on the adsorption of p-ASA. To further quantify the oxidation of ROX, the ratios of A_{400nm}–A_{244nm} ($R_{A400nm:A244nm}$) were calculated and their varying trends were illustrated (Fig. S6). After being adsorbed onto MnO_2, $R_{A400nm:A244nm}$ was observed to increase from 0.215 to 0.244 nm after 24.0 h contact time. In contrast, $R_{A400nm:A244nm}$ showed little change after the adsorption of ROX onto either FMBO or FeOOH, and the oxidation involved in was inferred to be rather weak. Additionally, the interaction between aromatic organoarsenic and Mn (IV) oxide was pH-dependent and the elevated pH inhibited the heterogeneous oxidation as indicated observed from UV–vis spectra.

Moreover, adsorption and oxidation process indicated that there was a formation of new intermediate during the adsorption of organic compounds onto Mn(IV)-based sorbents, resulting to the reductive dissolution of Mn(IV) [38]. MnO_2 exhibits oxidative surfaces towards various pollutants such as As(III) [39], phenol [40], and aniline [41]. Mn^{II} release from FMBO and MnO_2 was more significant at lower pH, and p-ASA showed higher efficacy to dissolve Mn(IV) than ROX (Fig. 5). Quantitatively, the concentrations of released Mn were as high as 16.9 and 6.0 mg L^{-1} after the adsorption of p-ASA onto MnO_2 and FMBO. At elevated pH 9.0, the much lowered concentrations of 0.43 and 0.39 mg L^{-1} was observed accordingly. The inhibited Mn^{II} release at higher pH was relative to the less extent of Mn(IV) dissolution.

Wang et al. (2015) investigated the oxidative and adsorptive behaviors of p-ASA on birnessite (δ-MnO_2), and reported the significance of heterogeneous oxidation effect in transformation of p-ASA and Mn^{II} release [13]. When p-ASA reacted with Mn(IV) oxide at pH 4.0, electron transfer from p-ASA to $\equiv Mn^{IV}OH$ occurred, which was converted into Mn^{III} could further reduce to Mn^{II}. The

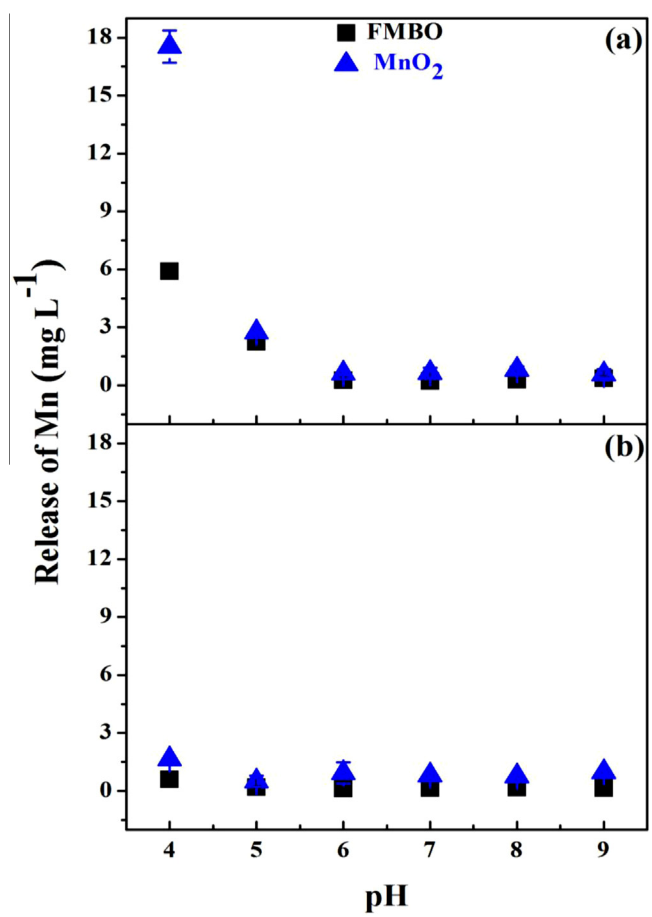

Fig. 5. Release of Mn from FMBO and MnO_2 after the adsorption of (a) p-ASA and (b) ROX.

possible p-ASA radical intermediate was occurred accordingly in Eq. (5) [13,42]. The reduction of Mn^{IV} to Mn^{II} may be simply expressed as Eq. (6).

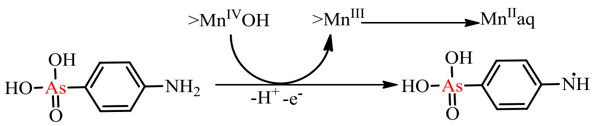

(5)

$$\frac{1}{2}MnO_2(s) + 2H^+ + e^- = \frac{1}{2}Mn^{II+}(aq) + H_2O \tag{6}$$

FMBO, with the molar ratio of Mn to Fe ($R_{Mn:Fe}$) of 1:3, showed less oxidative surface than MnO_2; however, the electrons transfer to Mn(IV) within FMBO also involved in. Additionally, the extent of p-ASA oxidation by FMBO was relatively lower than that by MnO_2, as indicated by lower concentrations of released Mn.

The adsorption of ROX also involved in the heterogeneous electrons transfer; however, the release of Mn from FMBO and MnO_2 was very low of 0.48 and 1.6 mg L^{-1} at pH 4.0. Ar-NH_2 group within p-ASA showed higher reductive activity towards Mn(IV) oxide as compared to the Ar-NO_2 group within ROX, and the more significant Mn release was observed thereafter. FMBO shows significantly higher adsorption capacity towards As(III) than As(V), and the oxidation of As(III) to As(V) is reported to play a significant role [24]. The oxidation transforms of non-ionic As(III) to negative As(V) with higher affinity to adsorbents; moreover, the reductive dissolution of FMBO provides more active sites available for As (V) adsorption [43].

The species transformation involved in the adsorption of p-ASA onto these adsorbents was further examined by UPLC-ICP-MS (Fig. 6). The decreased intensity was observed after the adsorption of p-ASA onto these three adsorbents, and the extent of decrease followed the trends of FMBO > FeOOH > MnO_2 (Fig. 6 inset). Interestingly, the interaction between p-ASA and MnO_2 contributed to the appearance of two peaks related to As(III) and As(V), respectively. However, no new peaks were observed after the adsorption of p-ASA onto FMBO and FeOOH even after 24.0 h reaction time.

The formation of inorganic arsenic is highly dependent on pH, and the lower pH benefits the oxidation of p-ASA by MnO_2 [13]. At relatively high pH 7.5, p-ASA can rarely be completely oxidized to arsenate and the arsenite peak can also be observed. During the adsorption of p-ASA onto MnO_2 at pH 7.5, p-ASA was first converted into arsenite and later oxidized into arsenate (Fig. 6). The pH-dependent oxidation of arsenite to arsenate by MnO_2 has been well investigated before [44,45].

FTIR spectra of p-ASA and ROX before and after their adsorption onto FMBO, FeOOH, and MnO_2 at pH 4.0 and 7.5 are illustrated in Fig. 7. A peak at 1630 cm^{-1} were assigned to the bending vibration of hydroxyl groups within water molecules on adsorbents surfaces [46]. The peaks (Fig. 7a) at 510 cm^{-1} and 525 cm^{-1} could be attributed to the bending vibration of Mn–O within FMBO and MnO_2 [47,48], and the band at 470 cm^{-1} corresponded to Fe–O vibration of FeOOH [49]. After adsorbing p-ASA and ROX, the peaks position shifted from 510 cm^{-1} to 530 cm^{-1} for FMBO, from 470 cm^{-1} to 450 cm^{-1} for FeOOH, and from 530 cm^{-1} and 525 cm^{-1} to 553 cm^{-1} and 450 cm^{-1} for MnO_2, respectively (Fig. 7). The significant variation in peaks position might be attributed to the attachment of p-ASA and ROX on their surfaces. Additionally, the peaks of p-ASA shifted from 1575 to 1590 cm^{-1} and from 1494 to 1503 cm^{-1} were observed after its being adsorbed onto FMBO, FeOOH, and MnO_2 at pH 4.0 (Fig. 7b). These peaks were assigned to N═Q═N stretching in the quinone ring and the C═C stretching vibration of aromatic amino moiety [50], owing to the protonation of the amine group under acidic condition [51]. The peaks at 1090 cm^{-1} and 1045 cm^{-1} were attributed to the stretching vibrations of the hydroxyl groups [21,50]. Furthermore, at lowered pH of 4.0, the new peaks at 830 cm^{-1} and 880 cm^{-1} were attributed to the vibration of the As–O band in p-ASA and ROX [21,52], and the appearance of these peak indicated their adsorption on surfaces. The weak peak at 880 cm^{-1} was observed after ROX adsorption onto FMBO at pH 4.0, and this was in accordance with the low adsorption capacity (Fig. 7c). The position of newly appeared peak was strongly dependent on pH, and the adsorption and oxidation were comparatively higher in pH 4.0 than that in pH 7.5.

To further identify the active sites for adsorption, the chemical states of Fe, Mn, and As were analyzed through XPS measurement. The full-scan XPS spectra of FMBO, FeOOH, and MnO_2, and those

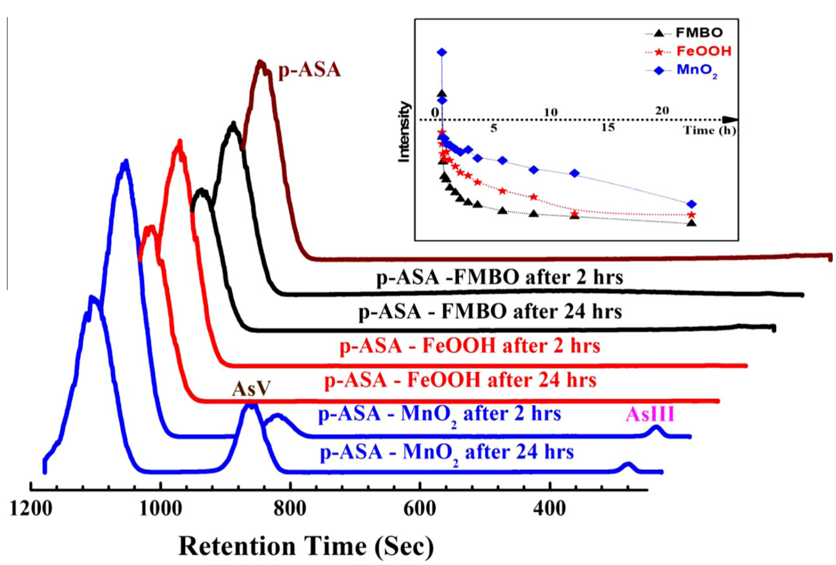

Fig. 6. Oxidative intermediates formation involve in the adsorption of p-ASA onto FMBO, FeOOH, and MnO_2 as indicated from UPLC-ICP-MS. Inset Figure display the decrease in intensity after adsorption.

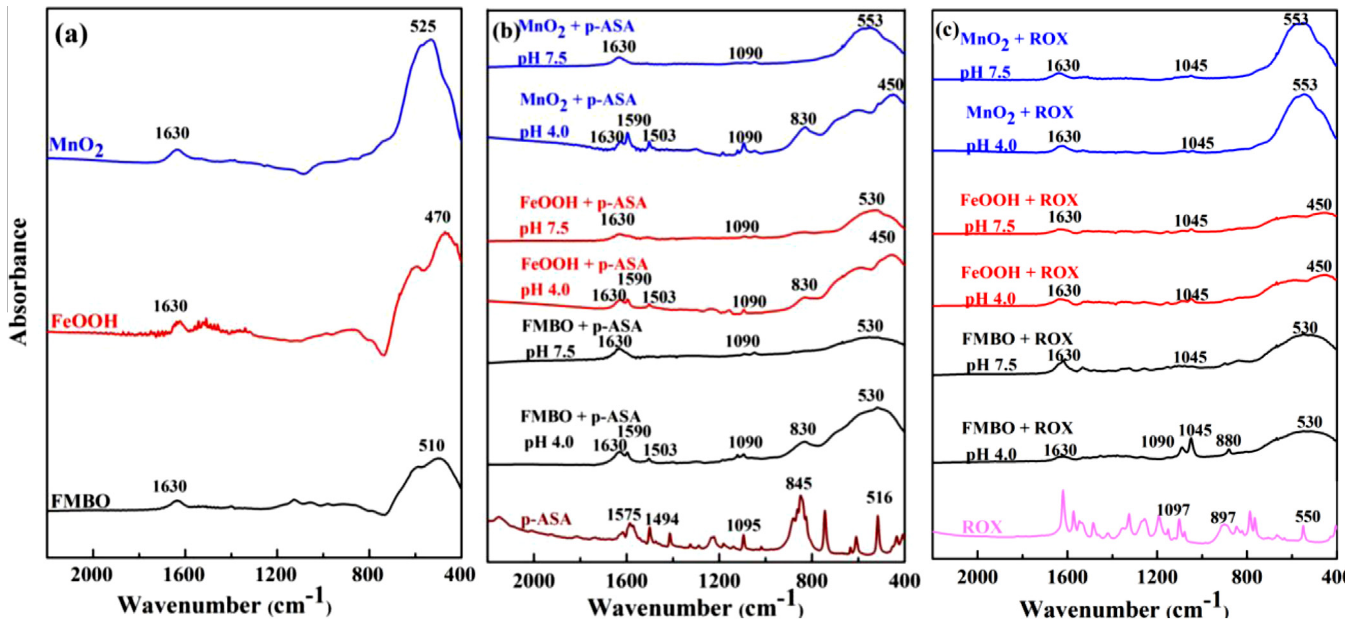

Fig. 7. FTIR spectra of (a) FMBO, FeOOH, and MnO_2, after the adsorption of (b) p-ASA, and (c) ROX.

with adsorbed p-ASA and ROX at pH 4.0 and 7.5 were illustrated in Figs. S7–S10. After adsorbing p-ASA and ROX, these adsorbents showed significantly changed surfaces in terms of full-scan XPS spectra. There appeared two new peaks at 45.0 eV (As 3d) and 398.2 eV (N 1S), and this indicated the adsorption of p-ASA and ROX on these surfaces. Fig. 8 illustrates As 3d core level spectra after the adsorption of p-ASA and ROX onto FMBO and MnO_2 at pH 4.0 and 7.5. There showed two new bands in binding energy (BE) range of 44.9–45.4 eV and 49.5–50.0 eV, which represented the As 3d and Mn 3p core levels [53]. Furthermore, the adsorption of p-ASA and ROX contributed to the appearance of the As 3d peak in BE range of 44.9–45.4 eV, and this peak was related to As(V) [54]. However, there showed no shift in BE of As 3d, and the pentavalent form, i.e., As(V), within p-ASA and ROX did not change after being adsorbed (Fig. S10 inset). Additionally, peak area of As 3d decreased with elevated pH from 4.0 to 7.5, and this was in accordance with the lowered adsorption at higher pH (Fig. 3). The Mn 2p of FMBO showed the BE of 642.6 and 654.1 eV and that of MnO_2 was observed to be 642.7 and 654.2 eV, and they could be attributed to Mn $2p_{3/2}$ and Mn $2p_{1/2}$ (Fig. S11A). The distance between these two peaks i.e., 11.5 eV, indicating the presence of Mn^{IV} ions [55,56]. After adsorption at pH 4.0, the atomic percentage of Mn was decreased in FMBO and MnO_2, that may be due to covering the surface by organoarsenic and the reductive dissolution of Mn(IV) within FMBO and MnO_2 at low pH as given in Table 2. As indicated from the fitted data and peak position, the BE of Mn $2p_{3/2}$ decreased after the adsorption of p-ASA on MnO_2 at pH 4.0, which demonstrated the reductive effect of p-ASA towards Mn(IV) within MnO_2 Eqs. (7)–(9) [13]. MnO_2 can first oxidize p-ASA and then transforms to MnOOH as shown in Eqs. (7) and (8). MnOOH also exhibited oxidative effects towards p-ASA and its intermediates, and Mn^{II} release occurred accordingly Eqs. (9) and (10). Furthermore, the release of Mn^{II} can further readsorbed onto the surface of Mn^{IV} oxide Eq. (11) [54,57]. According to the similar XPS results, it was reasonable to speculate that the organoarsenic oxidation mechanism on the surface of FMBO should be same as that of MnO_2.

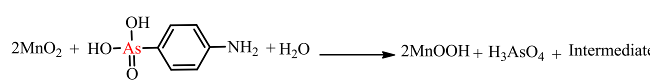

(7)

$$\text{Intermediate} + MnO_2 \rightarrow MnOOH + \text{Further Oxidation Product} \quad (8)$$

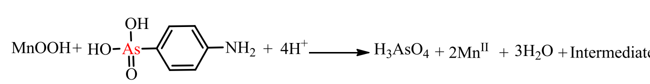

(9)

$$\text{Intermediate} + MnOOH \rightarrow Mn^{II} + \text{Further Oxidation Product} \quad (10)$$

$$2Mn^{II} + MnO_2 + 2H_2O \rightarrow 2MnOOH + 2H^+ \quad (11)$$

Considering the fact that small portion of the adsorbent was participated during the adsorption and oxidation process, which was reflected by the high removal efficiency after several recycles without any reduction of original efficiency (Fig. S12). The recyclability result exhibited that FMBO could be easily regenerated and has a good potential for the long-term stabilities of the adsorbents.

The dominant mechanisms involved in the adsorption of p-ASA and ROX onto FeOOH, which was indicated by XPS results. The atomic ratios of Fe content decreased, whereas As content increased after the adsorption of p-ASA and ROX (Table 2), and this supported that the Fe atoms were covered by the adsorbed p-ASA and ROX [58]. From this result, it was observed that FeOOH has sorption capacity and MnO_2 showed heterogeneous oxidation reaction. Thus, the synergism of Fe- and Mn-oxide dominates the high adsorption capacity of FMBO.

Thus, the underlying removal mechanism of p-ASA and ROX onto FMBO is proposed in Fig. 9. From the above results, during the initial step of reaction mechanism was adsorption through

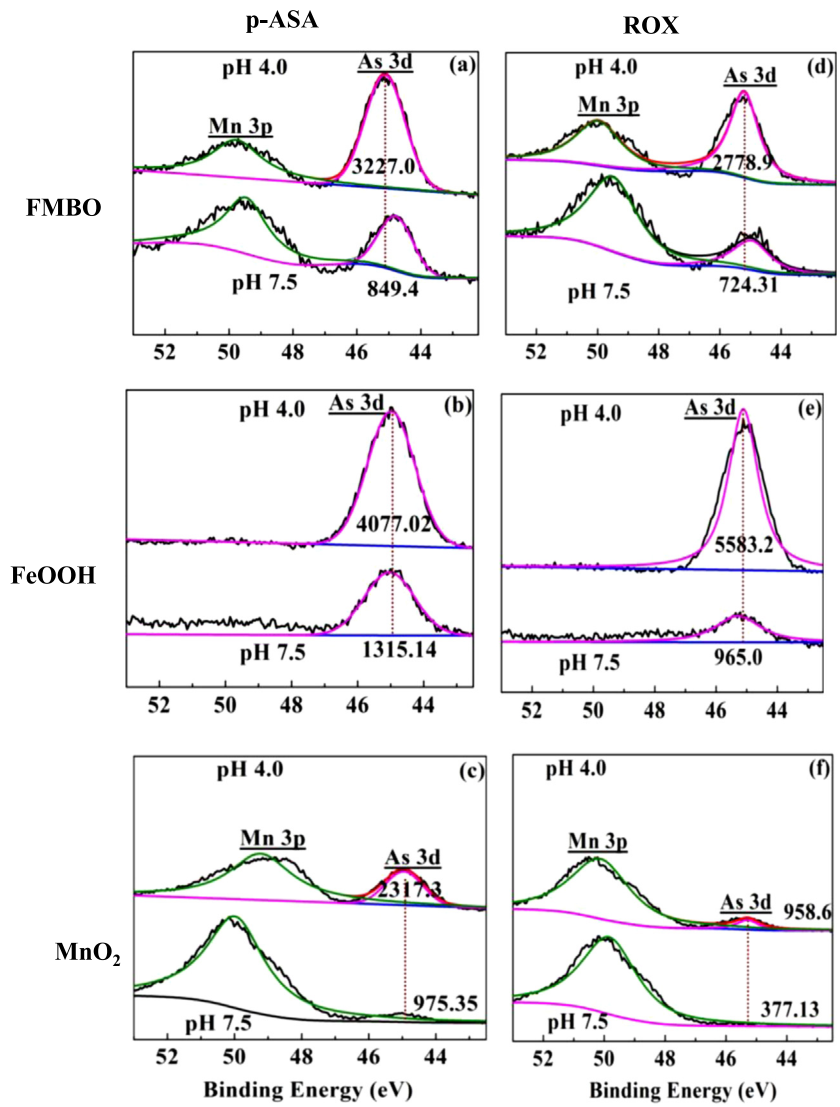

Fig. 8. As 3d core level photoelectron spectra of adsorption of (a, b, and c) p-ASA and (d, e, and f) ROX onto FMBO, FeOOH, and MnO_2. The number below the peak represents the peak area.

one electron transferred from p-ASA to Mn(IV) and a proton (H^+) was removed to form the inner-sphere complex as shown in Step-I and Step-II. These adsorbents tend to form ≡S—OH groups via protonation reactions, and exhibit pH dependent surface charges through surface dissolution and hydrolysis reactions. The adsorption of p-ASA and ROX onto ≡S—OH surfaces involved in several mechanisms of hydrogen bonding, electron donor, dipolar force, and electrostatic interaction [15–19]. FMBO, with the highest S_{BET} of 216 $m^2\ g^{-1}$, showed more lattice oxygen on its surface than the other two adsorbents, which also attributed to higher adsorption performance [59]. Furthermore, the Mn^{III} and Mn^{IV} locates in the center may accept one electron. This effect lead to hydrogen release and promoted the oxidation of organoarsenic and formation of radical intermediate, and the release of Mn^{II} occurred as described in step III, the reduction of Mn^{IV} to Mn^{II} was supported by the lowered BE of Mn 2p (Fig. S11A), indicated the elevated Mn^{II} concentrations after adsorption, which was readsorbed on the surface of adsorbents. On the basis of BE, Fe^{III} was identified as the core oxidation state in FMBO [24] (Fig. S11B). The formation of monodentate complex also occurred on the Fe^{III} surfaces with the removal of H^+, in Step-IV and Step-V. The higher adsorption capacity of p-ASA than that of ROX may be attributed to the $-NH_2$ group with stronger reductive effects. The dominant mechanisms involved in the adsorption of p-ASA and ROX were similar except that the stronger oxidation was observed for p-ASA (Step-VI to step X).

4. Conclusions

FMBO can be efficiently applied for organoarsenic compound removal from the aqueous solution. The synergism between Mn (IV) and Fe(III) oxides in FMBO enables its high affinity towards organoarsenic. In the adsorption of p-ASA and ROX onto FMBO, the heterogeneous oxidation converts the two organoarsenic species into intermediates, thereby the as-transformed arsenic was rapidly removed from the surface of ferric oxide. Results of Mn release, FTIR, and XPS spectra indicate more significant oxidation of organoarsenic at low pH. This effect benefits the adsorption of p-ASA and ROX and more significant adsorption was observed accordingly. These outcomes advances as the understanding of the removal efficiency and mechanism of organoarsenic, and for the development and optimization of adsorbents thereafter.

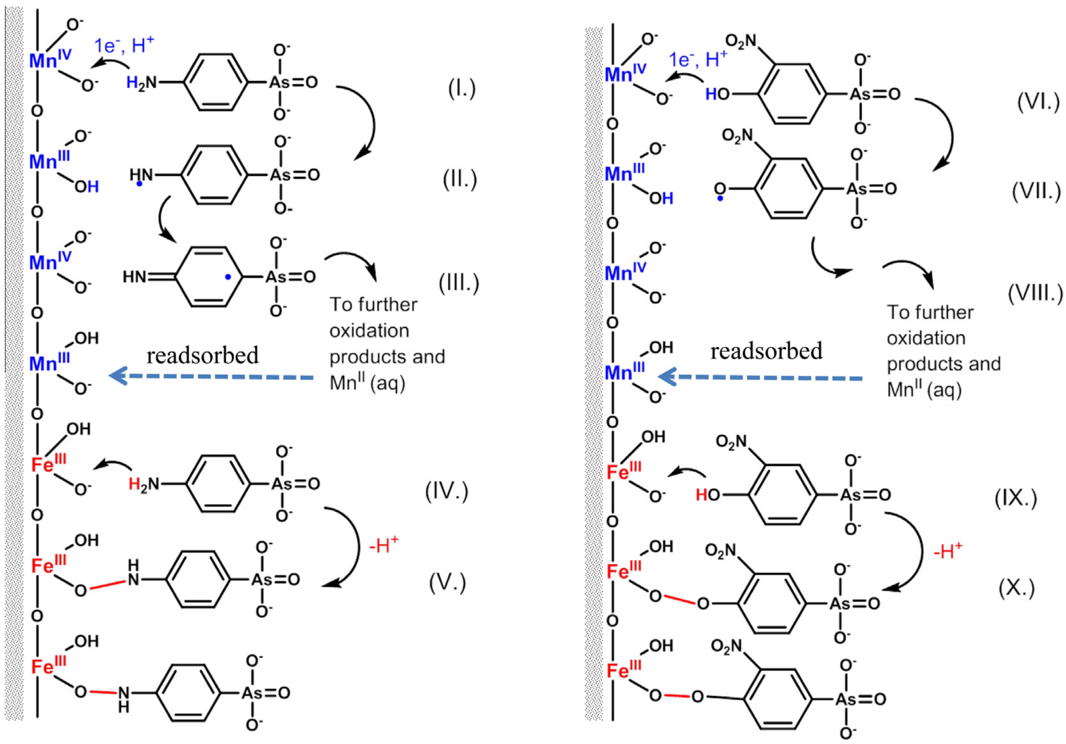

Fig. 9. Schematic diagram for the proposed removal mechanism of (a) p-ASA and (b) ROX onto FMBO.

Acknowledgements

This study was funded by the Natural Science Foundation of China (grant numbers 51422813, 512218920, 51378490).

Appendix A. Supplementary data

Supplementary data associated with this article can be found, in the online version, at http://dx.doi.org/10.1016/j.cej.2016.10.084.

References

[1] J.R. Garbarino, A.J. Bednar, D.W. Rutherford, R.S. Beyer, R.L. Wershaw, Environmental fate of roxarsone in poultry litter. I. Degradation of roxarsone during composting, Environ. Sci. Technol. 37 (2003) 1509–1514.
[2] H.D. Chapman, Z.B. Johnson, Use of antibiotics and roxarsone in broiler chickens in the USA: analysis for the years, to 2000, Poult. Sci. 81 (2002) (1995) 356–364.
[3] B.P. Jackson, P.M. Bertsch, Determination of arsenic speciation in poultry wastes by IC-ICP-MS, Environ. Sci. Technol. 35 (2001) 4868–4873.
[4] D.W. Rutherford, A.J. Bednar, J.R. Garbarino, R. Needham, K.W. Staver, R.L. Wershaw, Environmental fate of roxarsone in poultry litter part II. Mobility of arsenic in soils amended with poultry litter, Environ. Sci. Technol. 37 (2003) 1515–1520.
[5] J.F. Stolz, E. Perera, B. Kilonzo, B. Kail, B. Crable, E. Fisher, M. Ranganathan, L. Wormer, P. Basu, Biotransformation of 3-nitro-4-hydroxybenzene arsonic acid (roxarsone) and release of inorganic arsenic by *Clostridium* species, Environ. Sci. Technol. 41 (2007) 818–823.
[6] I. Cortinas, J.A. Field, M. Kopplin, J.R. Garbarino, A.J. Gandolfi, R. Sierra-Alvarez, Anaerobic biotransformation of roxarsone and related N-substituted phenylarsonic acids, Environ. Sci. Technol. 40 (2006) 2951–2957.
[7] D. Mohan, C.U. Pittman Jr., Arsenic removal from water/wastewater using adsorbents – a critical review, J. Hazard. Mater. 142 (2007) 1–53.
[8] Z.S. Veličković, Z.J. Bajić, M.Đ. Ristić, V.R. Djokić, A.D. Marinković, P.S. Uskoković, M.M. Vuruna, Modification of multi-wall carbon nanotubes for the removal of cadmium, lead and arsenic from wastewater, Dig. J. Nanomater. Biostruct. 8 (2013) 501–511.
[9] Z.J. Bajić, V.R. Djokić, Z.S. Veličkovivelikonić, M.M. Vuruna, M.D. Ristić, N. Ben Issa, A.D. Marinković, Equilibrium, kinetic and thermodynamic studies on removal of Cd(II), Pb(II) and As(V) from wastewater using carp (*Cyprinus carpio*) scales, Dig. J. Nanomater. Biostruct. 8 (2013) 1581–1590.
[10] B. Liu, M. Jian, R. Liu, J. Yao, X. Zhang, Highly efficient removal of arsenic(III) from aqueous solution by zeolitic imidazolate frameworks with different morphology, Colloids Surf. A: Physicochem. Eng. Aspects 481 (2015) 358–366.
[11] Z.J. Baji, Z.S. Veli, D. Kovi, V.R. Djoki, O. Ersen, P.S. Uskokovi, A.D. Marinkovi, Adsorption study of arsenic removal by novel hybrid copper impregnated tufa adsorbents in a batch system, Clean Soil Air Water (2016) 1–12.
[12] A. Jain, K.P. Raven, R.H. Loeppert, Arsenite and arsenate adsorption on ferrihydrite: surface charge reduction and net OH- release stoichiometry, Environ. Sci. Technol. 33 (1999) 1179–1184.
[13] L. Wang, H. Cheng, Birnessite (δ-MnO_2) mediated degradation of organoarsenic feed additive p-arsanilic acid, Environ. Sci. Technol. 49 (2015) 3473–3481.
[14] B.K. Jung, J.W. Jun, Z. Hasan, S.H. Jhung, Adsorptive removal of p-arsanilic acid from water using mesoporous zeolitic imidazolate framework-8, Chem. Eng. J. 267 (2015) 9–15.
[15] J.W. Jun, M. Tong, B.K. Jung, Z. Hasan, C. Zhong, S.H. Jhung, Effect of central metal ions of analogous metal-organic frameworks on adsorption of organoarsenic compounds from water: plausible mechanism of adsorption and water purification, Chem. Eur. J. 21 (2015) 347–354.
[16] J.J. Hu, Z. Tong, Z. Hu, G. Chen, T. Chen, Adsorption of roxarsone from aqueous solution by multi-walled carbon nanotubes, J. Colloid Interface Sci. 377 (2012) 355–361.
[17] J. Hu, Z. Tong, G. Chen, X. Zhan, Z. Hu, Adsorption of roxarsone by iron (hydr) oxide-modified multi-walled carbon nanotubes from aqueous solution and its mechanisms, Int. J. Environ. Sci. Technol. 11 (2014) 785–794.
[18] L. Poon, S. Younus, L.D. Wilson, Adsorption study of an organoarsenical with chitosan based sorbents, J. Colloid Interface Sci. 420 (2014) 136–144.
[19] W.R. Chen, C.H. Huang, Surface adsorption of organoarsenic roxarsone and arsanilic acid on iron and aluminum oxides, J. Hazard. Mater. 227–228 (2012) 378–385.
[20] S. Zheng, W. Jiang, Y. Cai, D.D. Dionysiou, K.E. O'Shea, Adsorption and photocatalytic degradation of aromatic organoarsenic compounds in TiO_2 suspension, Catal. Today 224 (2014) 83–88.
[21] G. Zhang, J. Qu, H. Liu, R. Liu, R. Wu, Preparation and evaluation of a novel Fe–Mn binary oxide adsorbent for effective arsenite removal, Water Res. 41 (2007) 1921–1928.
[22] H. Li, L.S. Lee, D.G. Schulze, C.A. Guest, Role of soil manganese in the oxidation of aromatic amines, Environ. Sci. Technol. 37 (2003) 2686–2693.
[23] S. Depalma, S. Cowen, T. Hoang, H.A. Al-Abadleh, Adsorption thermodynamics of p-arsanilic acid on iron (oxyhydr) oxides: in-situ ATR-FTIR studies, Environ. Sci. Technol. 42 (2008) 1922–1927.
[24] W. Xu, H. Wang, R. Liu, X. Zhao, J. Qu, The mechanism of antimony(III) removal and its reactions on the surfaces of Fe–Mn binary oxide, J. Colloid Interface Sci. 363 (2011) 320–326.
[25] R. Liu, W. Xu, Z. He, H. Lan, H. Liu, J. Qu, T. Prasai, Adsorption of antimony(V) onto Mn(II)-enriched surfaces of manganese-oxide and FeMn binary oxide, Chemosphere 138 (2015) 616–624.

[26] J. Zheng, A. Iijima, N. Furuta, Complexation effect of antimony compounds with citric acid and its application to the speciation of antimony(III) and antimony(V) using HPLC-ICP-MS, J. Anal. At. Spectr. 16 (2001) 812–818.
[27] G. Zhang, M. Sun, Y. Liu, X. Lang, L. Liu, H. Liu, J. Qu, J. Li, Visible-light induced photocatalytic activity of electrospun-TiO_2 in arsenic(III) oxidation, ACS Appl. Mater. Interfaces 7 (2015) 511–518.
[28] I.S. Mclintock, The Elovich equation in chemisorption kinetics, Nature 216 (1967) 1204–1205.
[29] M. Jian, B. Liu, G. Zhang, R. Liu, X. Zhang, Adsorptive removal of arsenic from aqueous solution by zeolitic imidazolate framework-8 (ZIF-8) nanoparticles, Colloids Surf. A: Physicochem. Eng. Aspects 465 (2015) 67–76.
[30] J.A. Pedit, C.T. Miller, Heterogeneous sorption processes in subsurface systems. 1. Model formulations and applications, Environ. Sci. Technol. 28 (1994) 2094–2104.
[31] K.Y. Foo, B.H. Hameed, Insights into the modeling of adsorption isotherm systems, Chem. Eng. J. 156 (2010) 2–10.
[32] H. Zhang, C.H. Huang, Oxidative transformation of triclosan and chlorophene by manganese oxides, Environ. Sci. Technol. 37 (2003) 2421–2430.
[33] R. Liu, F. Liu, C. Hu, Z. He, H. Liu, J. Qu, Simultaneous removal of Cd(II) and Sb(V) by Fe–Mn binary oxide: positive effects of Cd(II) on Sb(V) adsorption, J. Hazard. Mater. 300 (2015) 847–854.
[34] D.A. Sverjensky, K. Fukushi, A predictive model (ETLM) for As(III) adsorption and surface speciation on oxides consistent with spectroscopic data, Geochim. Cosmochim. Acta 3778–3802 (2006).
[35] W. Stumn, Chemistry of the Solid-Water Interface, John Wiley & Sons Inc., 1992.
[36] X.D. Zhu, Y.J. Wang, C. Liu, W.X. Qin, D.M. Zhou, Kinetics, intermediates and acute toxicity of arsanilic acid photolysis, Chemosphere 107 (2014) 274–281.
[37] Z. Cheng, J. Liao, B. He, F. Zhang, F. Zhang, X. Huang, L. Zhou, One-step fabrication of graphene oxide enhanced magnetic composite gel for highly efficient dye adsorption and catalysis, ACS Sustainable Chem. 3 (2015) 1677–1685.
[38] Y. Wang, A.T. Stone, Reaction of MnIII, IV (hydr)oxides with oxalic acid, glyoxylic acid, phosphonoformic acid, and structurally-related organic compounds, Geochim. Cosmochim. Acta 70 (2006) 4477–4490.
[39] B.J. Lafferty, M. Ginder-Vogel, D.L. Sparks, Arsenite oxidation by a poorly crystalline manganese-oxide 1. Stirred-flow experiments, Environ. Sci. Technol. 44 (2010) 8460–8466.
[40] A.T. Stone, Reductive dissolution of manganese (III/IV) oxides by substituted phenols, Environ. Sci. Technol. 21 (1987) 979–988.
[41] S. Laha, R.G. Luthy, Oxidation of aniline and other primary aromatic amines by manganese dioxide, Environ. Sci. Technol. 24 (1990) 363–373.
[42] H. Zhang, C.H. Huang, Oxidative transformation of fluoroquinolone antibacterial agents and structurally related amines by manganese oxide, Environ. Sci. Technol. 39 (2005) 4474–4483.
[43] G. Zhang, H. Liu, R. Liu, J. Qu, Removal of phosphate from water by a Fe–Mn binary oxide adsorbent, J. Colloid Interface Sci. 335 (2009) 168–174.
[44] B.J. Lafferty, G.V. Matthew, Z. Mengqiang, K.J.T. Livi, D.L. Sparks, Arsenite oxidation by a poorly crystalline manganese-oxide. 2. Results from x-ray absorption spectroscopy and x-ray diffraction, Environ. Sci. Technol. 44 (2010) 8467–8472.
[45] B.A. Manning, S.E. Fendorf, B. Benjamin, D.L. Suarez, Arsenic(III) oxidation and arsenic(V) adsorption reactions on synthetic birnessite, Environ. Sci. Technol. 36 (2002) 976–981.
[46] G. Zhang, H. Liu, R. Liu, J. Qu, Adsorption behavior and mechanism of arsenate at Fe–Mn binary oxide/water interface, J. Hazard. Mater. 168 (2009) 820–825.
[47] P. Hu, Y. Liu, B. Jiang, X. Zheng, J. Zheng, M. Wu, High-efficiency simultaneous oxidation of organoarsenic and immobilization of arsenic in Fenton enhanced plasma system, Ind. Eng. Chem. Res. 8277–8286 (2015).
[48] Y. Ren, N. Yan, J. Feng, J. Ma, Q. Wen, N. Li, Q. Dong, Adsorption mechanism of copper and lead ions onto graphene nanosheet/δ-MnO_2, Mater. Chem. Phys. 136 (2012) 538–544.
[49] S.A. Baig, T. Sheng, C. Sun, X. Xue, L. Tan, X. Xu, Arsenic removal from aqueous solutions using Fe_3O_4-HBC composite: effect of calcination on adsorbents performance, PLoS ONE 9 (2014) e100704.
[50] G. Chen, L. Zhao, Y.H. Dong, Oxidative degradation kinetics and products of chlortetracycline by manganese dioxide, J. Hazard. Mater. 193 (2011) 128–138.
[51] M. Czaplicka, L. Bratek, K. Jaworek, J. Bonarski, S. Pawlak, Photo-oxidation of p-arsanilic acid in acidic solutions: kinetics and the identification of by-products and reaction pathways, Chem. Eng. J. 243 (2014) 364–371.
[52] P. Maria, M. Xiaoguang, G.P. Korfiatis, J. Chuanyong, Adsorption mechanism of arsenic on nanocrystalline titanium dioxide, Environ. Sci. Technol. 40 (2006) 1257–1262.
[53] S. Ouvrard, P. de Donato, M.O. Simonnot, S. Begin, J. Ghanbaja, M. Alnot, Y.B. Duval, F. Lhote, O. Barres, M. Sardin, Natural manganese oxide: combined analytical approach for solid characterization and arsenic retention, Geochim. Cosmochim. Acta 69 (2005) 2715–2724.
[54] H.W. Nesbitt, G.W. Canning, G.M. Bancroft, XPS study of reductive dissolution of 7 Å-birnessite by H_3AsO_3, with constraints on reaction mechanism, Geochim. Cosmochim. Acta 62 (1998) 2097–2110.
[55] G. Han, Y. Liu, L. Zhang, E. Kan, S. Zhang, J. Tang, W. Tang, MnO_2 nanorods intercalating graphene oxide/polyaniline ternary composites for robust high-performance supercapacitors, Sci. Rep. 4 (2014) 1–7.
[56] M.C. Biesinger, B.P. Payne, A.P. Grosvenor, L.W.M. Lau, A.R. Gerson, R.S.C. Smart, Resolving surface chemical states in XPS analysis of first row transition metals, oxides and hydroxides: Cr, Mn, Fe, Co and Ni, Appl. Surf. Sci. 257 (2011) 2717–2730.
[57] G. Zhang, F. Liu, H. Liu, J. Qu, R. Liu, Respective role of Fe and Mn oxide contents for arsenic sorption in iron and manganese binary oxide: an x-ray absorption spectroscopy investigation, Environ. Sci. Technol. 48 (2014) 10316–10322.
[58] Y. Zhang, M. Yang, X.M. Dou, H. He, D.S. Wang, Arsenate adsorption on an Fe–Ce bimetal oxide adsorbent: role of surface properties, Environ. Sci. Technol. 39 (2005) 7246–7253.
[59] H. Sung Cho, H. Deng, K. Miyasaka, Z. Dong, M. Cho, A.V. Neimark, J. Ku Kang, O. M. Yaghi, O. Terasaki, Extra adsorption and adsorbate super lattice formation in metal-organic frameworks, Nature 527 (2015) 503–507.